electronics

MDPI

Article

Analysis and Design of a ZVT Resonant Boost Converter Using an Auxiliary Resonant Circuit

Hee-Jun Lee and Young-Ho Kim *

Department of Electrical and Computer Engineering, Sungkyunkwan University, Suwon 16419, Korea; jun9489@gmail.com

* Correspondence: toemtio@gmail.com; Tel.: +82-10-7124-5378

Received: 2 April 2019; Accepted: 22 April 2019; Published: 25 April 2019

Abstract: In this paper, a new zero voltage transition (ZVT) resonant boost converter is proposed. A typical boost converter generates switching losses at turning on and turning off, and these losses cause a reduction in the efficiency of the whole system. This proposed ZVT resonant boost converter utilizes a soft switching method, using an auxiliary circuit with a resonant inductor, capacitor, and two auxiliary switches. Therefore, it can reduce switching losses more so than the conventional hard switching converter. Also, the conduction period of the resonant inductor current is reduced by using a modified circuit. An experiment is conducted with the converter, which steps up the voltage from 200 V to 380 V and its switching frequency and output power are 30 kHz and 4 kW, respectively. It is confirmed that the experimental results and simulation results are the same and the validity of this proposed converter is verified. The conventional converter and proposed converter are analyzed by comparing the experimental results of two converters under the same conditions. It is confirmed that all switches can achieve soft switching and the proposed converter improves on the conventional converter by measuring the efficiency of two converters.

Keywords: zero voltage transition; boost converter; soft switching; auxiliary resonant circuit; zero voltage switching; zero current switching

1. Introduction

There has been an increase in the interest of using renewable energy sources to replace fossil fuels in order to resolve problems related to environmental destruction and to combat climate change and extreme weather trends that may be caused by environmental and air pollution that have resulted from recent rapid industrialization [1,2].

Various potential sources of alternate energy, including solar, wind, tidal, and hydrogen energy, have been the subject of intensive research. One of the disadvantages of using fuel cells and photovoltaic solar cells is that they have very low efficiency. Thus, it is very important to improve the efficiency of power conversion systems. As a result, much research has been undertaken to improve the efficiency of DC–DC converters [3–5].

A high switching frequency is required in the design of DC–DC converters that have a compact [6–8]. Non-ideal switching elements in hard switching converters cause switching losses because voltage and current are superimposed during switching and the higher the switching frequency, the greater the switching losses. These losses can be reduced through the use of soft switching. Many research papers on soft-switched resonant DC–DC converters with zero voltage switching (ZVS) and zero current switching (ZCS) techniques have been published, and several techniques that reduce switching losses have been proposed [9,10]. A Zero Current Transition (ZCT) converter can achieve ZCS using an auxiliary circuit, where the resonance conditions are not affected by variations in the load [11]. But the switching losses occur during the ZCT turn-off by the reverse recovery current. The current stress of the main switch and the conduction losses increase, since part of the current through the resonant inductor flow through the main switch. A zero voltage transition (ZVT) converter has an advantage where ZVS and ZCS can be achieved for a wide load range by using an auxiliary circuit [12–14].

A ZVT converter is used with a resonant inductor and capacitor to satisfy the ZVT condition. A resonant inductor through current is a reactive current because the resonance energy does not have a significant effect on the output and a resonant inductor is high current because the resonant current and the reactive current are the same. Thus, a highly resonant current increases losses of passive and active devices and the overall system efficiency is reduced.

In a conventional converter, the resonant inductor current flows continuously through the auxiliary circuit. Thus, the proposed ZVT Boost converter has a modified resonant circuit to reduce conduction loss.

This paper proposes a resonant ZVT boost DC–DC converter that uses an auxiliary resonant circuit to reduce switching losses and to improve converter efficiency. The resonant circuit is composed of a resonant inductor, a resonant capacitor, and an auxiliary switch. The auxiliary circuit is used in this converter to implement a soft-switching method. The switch of the auxiliary circuit also performs a soft-switching method through the resonant circuit. Furthermore, the conduction period of the resonant inductor is reduced using a modified circuit. And this leads to a reduction in the switching losses and an improvement in the overall system efficiency, as compared to a conventional converter at the same frequency.

2. Resonant Boost DC–DC Converter

2.1. ZVT Resonant Boost Converter

Figure 1a shows a conventional resonant ZVT boost converter. Its auxiliary circuit is composed of a boost converter, an auxiliary switch, a resonant inductor, two resonant capacitors, and two diodes. The resonant capacitor is discharged before the current flows through the body diode. These resonant components make a partial resonant path for the main switch to perform soft switching under the ZVT, using the resonant circuit [15]. However, the freewheeling period of the resonant inductor current causes a conduction loss of the diode and resonant inductor. This causes a reduction in the whole system's efficiency.

Figure 1b shows the proposed resonant ZVT boost converter. The converter is composed of a boost converter, a main inductor, two auxiliary switches, a resonant capacitor, and an auxiliary circuit with an auxiliary capacitor. The conduction period of the resonant inductor is reduced, using a modified circuit. And this leads to a reduction in the switching losses and an improvement in the overall system efficiency.

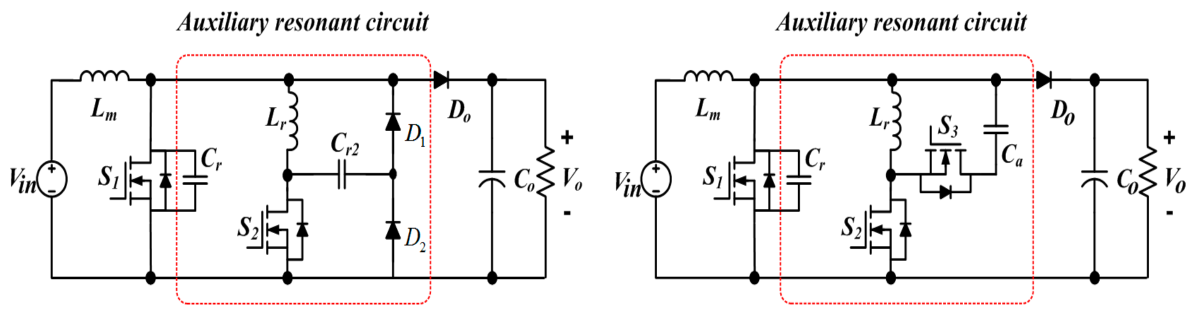

(a) (b)

Figure 1. (**a**) Conventional zero voltage transition (ZVT) resonant boost converter and (**b**) proposed ZVT resonant boost converter.

Figure 2 shows each waveform of the resonant inductor voltage and current for the conventional and proposed converter. The current conduction period of the proposed converter shown in Figure 2b is shorter than the conventional converter shown in Figure 2a.

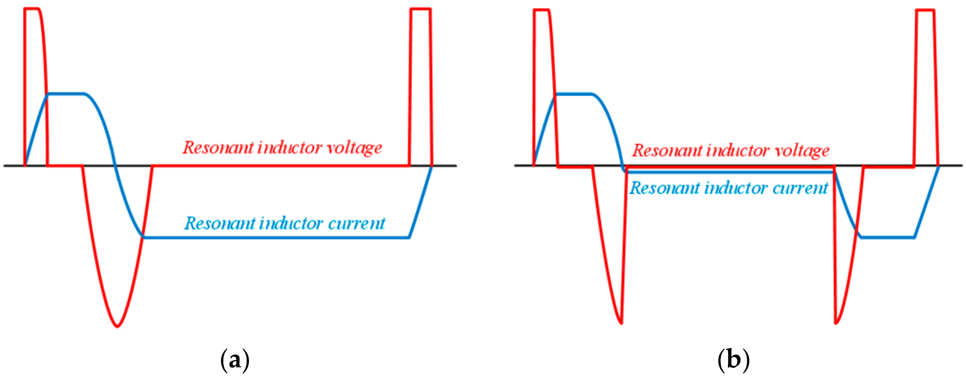

Figure 2. Comparison of resonant inductor current/voltage. (**a**) Conventional converter and (**b**) proposed converter.

2.2. Analysis of Proposed Converter

Operation mode of the proposed ZVT resonant boost converter is shown in Figure 3. The operational principle of the proposed converter is divided into ten modes for simple analysis. The mode 1, mode 2 and mode 10 are discharging mode of the proposed ZVT boost converter. The mode 4 made to satisfy the ZVT condition of the main switch S_1. And next Mode 5 is turned on under the ZVS condition. And the main inductor charges form mode 5 to mode 9. The mode 3, mode 5, mode 7 and mode 9 operate with resonance. The mode 2, mode 5 and mode 7 are turned on the soft switching of the auxiliary switches.

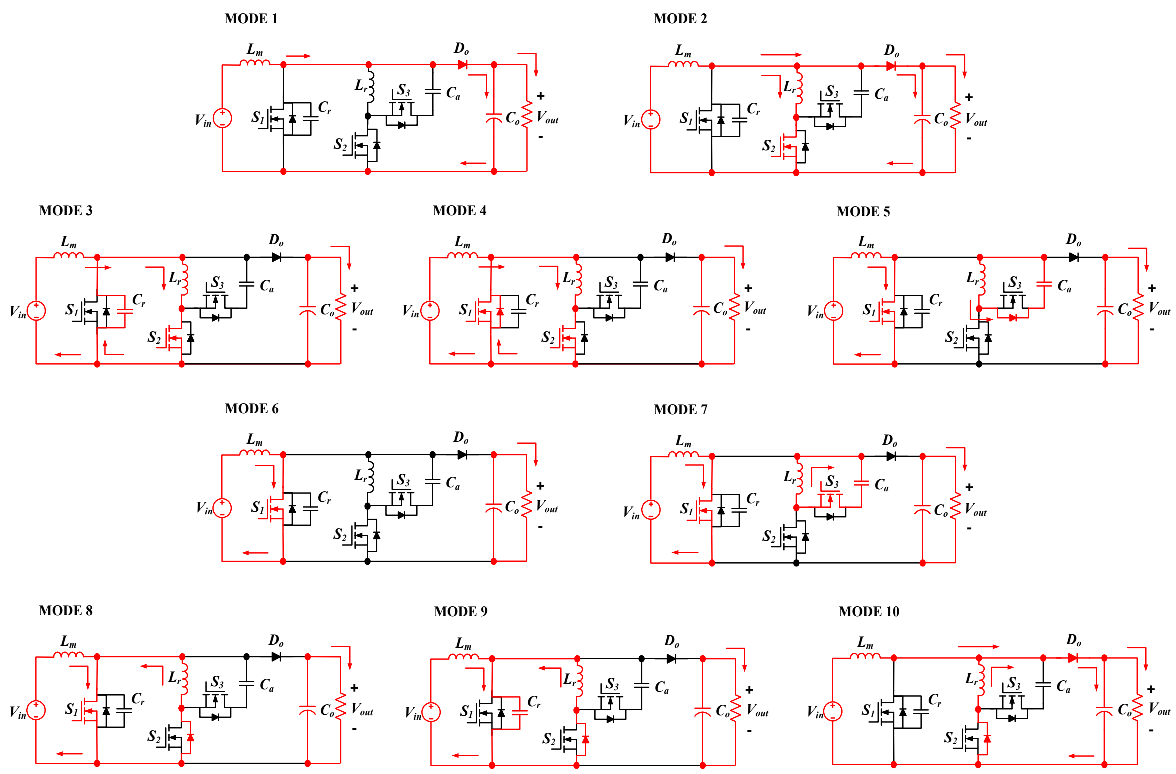

Figure 3. Operation mode of the proposed ZVT resonant boost converter.

The following statements are assumptions for simple analysis of the proposed converter: First, all switching devices and passive elements (inductor and capacitor) are ideal. Second, the input voltage 200 V and output voltage 380 V are constant. Third, the recovery time of all diodes is ignored. The resonant ZVT boost converters operate in 10 different modes, and the following assumptions were made for a steady-state analysis:

Mode 1 (t_0–t_1): Main S_1 and auxiliary switches S_2 and S_3 are turned off. The accumulated main inductor current L_m is flowed through the output diode D_o. Then, output and resonant capacitors C_o C_r are charged the same voltage. Equivalent circuit of mode 1 and key waveform is shown in Figure 4. The equivalent circuit shows when the main inductor discharges for boost.

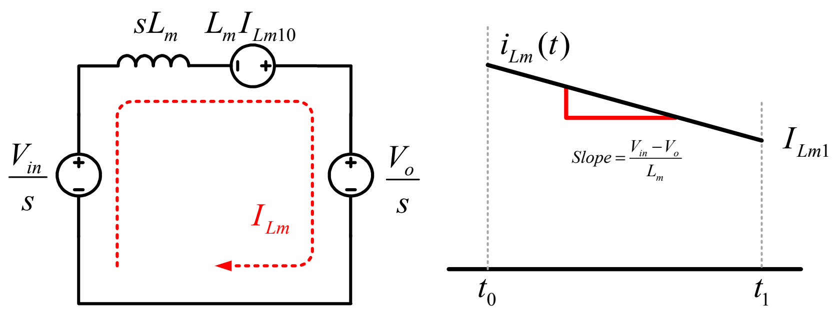

Figure 4. Equivalent circuit of Mode 1 and key waveform.

In Mode 1, the main inductor current i_{Lm} decreases and the resonant inductor current i_{Lr} and auxiliary capacitor voltage v_{Ca} are zero. This is expressed as the Equations (1) and (2).

$$i_{Lm}(t) = I_{Lm10} - \frac{V_{in} - V_o}{L_m}(t_0 - t_1) \tag{1}$$

$$i_{Lr}(t) = 0,\ v_{Cr}(t) = V_o,\ v_{Ca}(t) = 0 \tag{2}$$

Furthermore, the main inductor current I_{Lm1} is defined for the next mode t_2 analysis.

$$i_{Lm}(t_1) = I_{Lm1} \tag{3}$$

Mode 2 ($t_1 < t < t_2$): In Mode 2, an auxiliary switch S_2 turns on under the ZCS condition. The resonant inductor current i_{Lr} increases linearly from zero. The main inductor current i_{Lm} decreases. When the resonant inductor current i_{Lr} is equal to the main inductor current i_{Lm}, Mode 2 is completed. Also Figure 5 shows an equivalent circuit and key waveform for analyzing mode 2. And the Equivalent circuit Indicates to calculate the magnitude of the current of main inductor i_{Lm} and resonant inductor i_{Lr}. Thus, the main inductor current is equal to the minimum. The main inductor current i_{Lm} and resonant inductor current i_{Lr} are expressed by Equations (4) and (5).

$$i_{Lm}(t) = I_{Lm1} - \frac{V_o - V_{in}}{L_m}t,\ i_{Lr}(t) = \frac{V_o}{L_r}t \tag{4}$$

$$i_{Lm}(t_2) = i_{Lr}(t_2) \approx I_{min} \tag{5}$$

The resonant capacitor voltage v_{Cr} is equal to output voltage. If parasitic capacitance of resonant switch S_3 is ignored, auxiliary capacitor voltage v_{Ca} is zero.

$$v_{Cr}(t) = V_o,\ v_{Ca}(t) = 0 \tag{6}$$

For Mode 3, the resonant inductor current I_{Lr2} is defined as Equation (7).

$$i_{Lr}(t_2) = \frac{V_o}{L_r}t = I_{Lr2} = I_{Lm2} \tag{7}$$

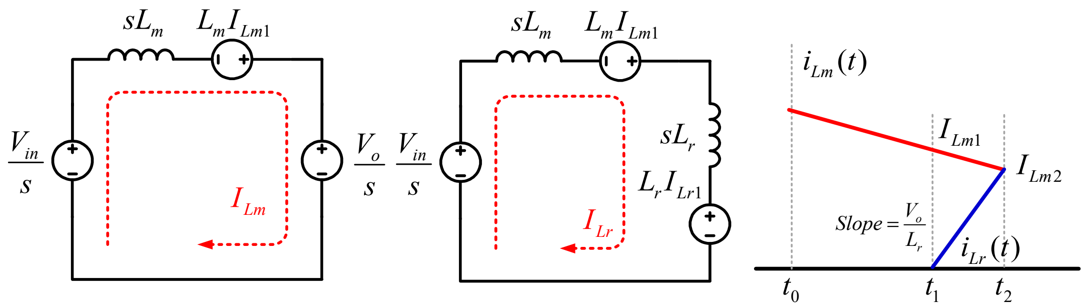

Figure 5. The equivalent circuit of Mode 2 and key waveform.

Mode 3 ($t_2 < t < t_3$): When the main and resonant inductor currents i_{Lm} and i_{Lr} are equalized, the resonance operation between resonant capacitor C_r and resonant inductor L_r is started. Then, output diode D_o is turned off because the resonant capacitor C_r is discharged. Then, equivalent circuit of resonance operation is shown in Figure 6. The key waveform of mode 3 indicates main inductor current i_{Lm}, resonant inductor current i_{Lr} and resonant capacitor voltage v_{Cr}.

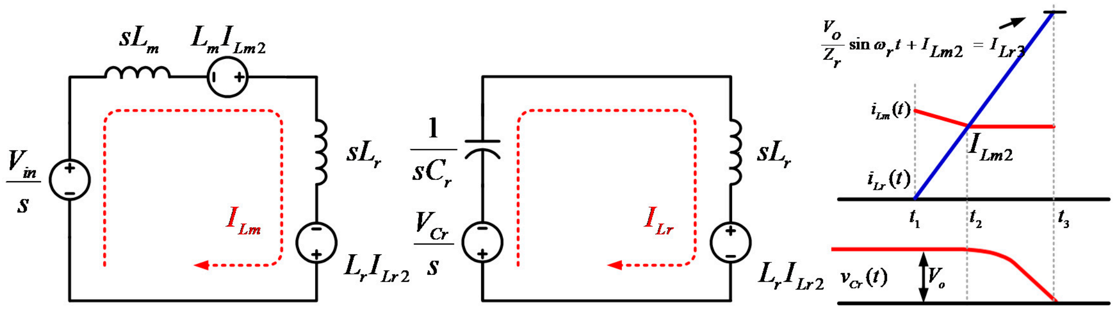

Figure 6. The equivalent circuit of Mode 3 and key waveform.

At the end of Mode 3, the resonant capacitor C_r is equal to zero. The resonant capacitor voltage v_{Cr} and resonant inductor current i_{Lr} can be obtained by the Laplace transform, following Equations (9), (10), (12), and (13). In addition, the resonant impedance Z_r and angular frequency ω_r are given by Equation (16). Additionally, i_{Lm}, i_{Lr}, v_{Ca}, and v_{Cr} are defined by Equations (8), (11), (14), and (15).

$$i_{Lm}(t) \approx I_{min} \tag{8}$$

$$\frac{V_o}{s} = \frac{i_{Lr}(s)}{sC_r} + sL_r i_{Lr}(s) + I_{min} \tag{9}$$

$$i_{Lr}(s) = \frac{\frac{V_o}{L_r}\sqrt{L_rC_r} \cdot \frac{1}{\sqrt{L_rC_r}}}{s^2 + \left(\frac{1}{\sqrt{L_rC_r}}\right)^2} + I_{min} \tag{10}$$

$$i_{Lr}(t) = \frac{V_o}{Z_r} sin\omega_r t + I_{min} \tag{11}$$

$$C_rV_o = sC_r v_{cr}(s) + \frac{vL_{Cr}(s)}{sL_r} \tag{12}$$

$$\begin{aligned} v_{Cr}(s) &= \frac{1}{sC_r + \frac{1}{sL_r}} C_rV_o \\ &= \frac{s}{s^2 + \left(\frac{1}{\sqrt{L_rC_r}}\right)^2} V_o \end{aligned} \tag{13}$$

$$v_{Cr}(t) = V_o cos\omega_r t \tag{14}$$

$$v_{Ca}(t) = 0 \tag{15}$$

where

$$\omega_r = \frac{1}{\sqrt{L_r C_r}}, Z_r = \sqrt{\frac{L_r}{C_r}} \tag{16}$$

The resonant inductor current I_{Lr3} is defined for the next mode t_4 analysis.

$$i_{Lr}(t_3) = \frac{V_o}{Z_r} sin\omega_r t + I_{Lr2} = I_{Lr3} \tag{17}$$

Mode 4 ($t_3 < t < t_4$): The body diode of the main switch S_1 is turned on, and the voltage of main switch S_1 is equal to zero. Then, the main switch S_1 is made to satisfy the ZVT condition. Resonant current flows through the anti-parallel diode of the main switch S_1. The main inductor current i_{Lm} and the resonant inductor current i_{Lr} can be derived from Equation (18). Auxiliary and resonant capacitor voltage v_{Cr} are all zero by Equation (19). Thus, Figure 7 shows for derivation of the equation. And voltage and current of switches is shown in the key waveform. Mode 4 ends when the auxiliary switch S_2 is turned off.

$$i_{Lm}(t) = \frac{V_{in}}{L_m} t + I_{min},\ i_{Lr}(t) = I_{Lr3} \tag{18}$$

$$v_{Cr}(t) = 0,\ v_{Ca}(t) = 0 \tag{19}$$

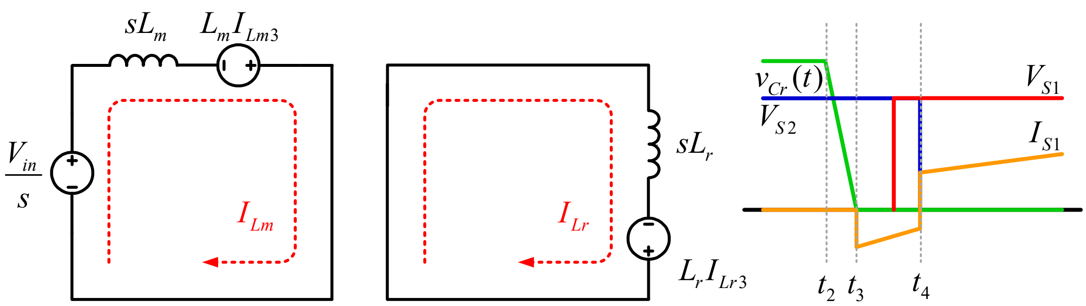

Figure 7. The equivalent circuit of Mode 4 and key waveform.

Main inductor current I_{Lm4} is defined for the next mode t_5 analysis.

$$i_{Lm}(t_4) = \frac{V_{in}}{L_m} t + i_{Lm3} = I_{Lm4} \tag{20}$$

Mode 5 ($t_4 < t < t_5$): In Mode 5, the main switch S_1 is turned on under the ZVS condition. Then, the main inductor current i_{Lm} increases linearly. The auxiliary switch S_2 is turned off in the same condition, while the second resonance is begun by the resonant inductor L_r and auxiliary capacitor C_a. Thus, the resonant inductor current i_{Lr} decreases. The auxiliary capacitor voltage v_{Ca} and resonant inductor current i_{Lr} can be derived from the Laplace transform, following Equations (22), (24), and (25). At this time, the equivalent circuit of mode 5 is shown in Figure 8. The equivalent circuit is divided into main inductor current i_{Lm} and resonance circuit. The key waveform indicates resonant inductor current i_{Lr}, main inductor current i_{Lm} and auxiliary capacitor voltage v_{Ca}.

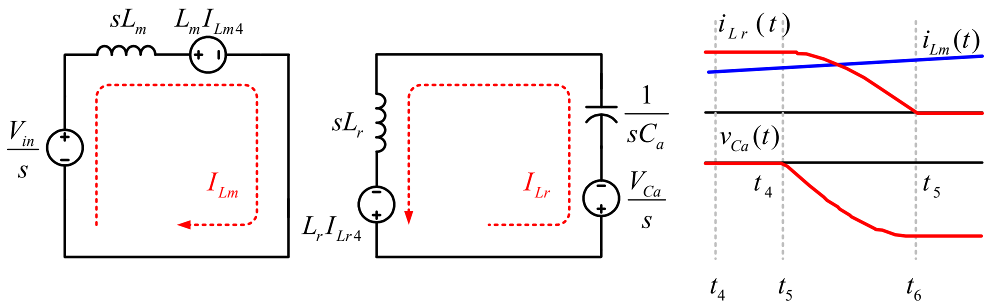

Figure 8. The equivalent circuit of Mode 5 and key waveform.

Additionally, the resonant impedance Z_a and angular frequency ω_a are given by Equation (27). Then, i_{Lm}, i_{Lr}, v_{ca}, and v_{Cr} are defined by Equations (21), (23), and (26).

$$i_{Lm}(t) = \frac{V_{in}}{L_m}t + I_{Lm4} \tag{21}$$

$$\begin{aligned} i_{Lr}(s) &= \frac{L_r I_{Lr4}}{\frac{1}{sC_a}+sL_r} \\ &= \frac{s}{s^2+\left(\frac{1}{\sqrt{L_r C_r}}\right)^2} I_{Lr4} \end{aligned} \tag{22}$$

$$i_{Lr}(t) = I_{Lr4} cos\omega_a t \tag{23}$$

$$\frac{I_{Lr4}}{s} = -\frac{v_{Ca}}{sL_r} + v_{Ca} sC_a \tag{24}$$

$$v_{Ca}(s) = -\frac{\sqrt{\frac{L_r}{C_a}} \cdot \frac{1}{\sqrt{L_r C_a}}}{s^2 + \left(\frac{1}{\sqrt{L_r C_a}}\right)^2} I_{Lr4} \tag{25}$$

$$v_{Ca}(t) = -Z_a I_{Lr4} sin\omega_a t \tag{26}$$

where

$$\omega_a = \frac{1}{\sqrt{L_r C_a}} Z_a = \sqrt{\frac{L_r}{C_a}} \tag{27}$$

For Mode 6, the resonant inductor current i_{Lr} and auxiliary capacitor voltage v_{Ca} are defined as Equation (28).

$$i_{Lr}(t_5) = 0 = I_{Lr5},\ v_{Ca}(t_5) \approx V_o \tag{28}$$

Mode 6 ($t_5 < t < t_6$): In Mode 6, resonant inductor L_r and auxiliary capacitor C_a end the second resonant operation and the resonant capacitor C_a is charged. The main inductor current i_{Lm} increases linearly through the main switch S_1. Mode 6 ends when the auxiliary switch S_3 turns on. The equivalent circuit of mode 6 and key waveform is shown in Figure 9. The main inductor current i_{Lm} can be calculated through the equivalent circuit. The i_{Lm}, i_{Lr}, v_{Ca}, and v_{Cr} values are as follows in Equations (29) and (30):

$$i_{Lm}(t) = \frac{V_{in}}{L_m}t + I_{Lm5},\ i_{Lr}(t) = 0 \tag{29}$$

$$v_{Ca}(t) = -V_o,\ v_{Cr}(t) = 0 \tag{30}$$

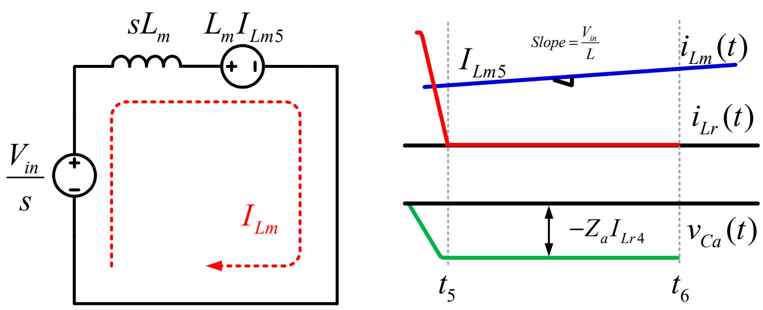

Figure 9. The equivalent circuit of Mode 6 and key waveform.

Mode 7 ($t_6 < t < t_7$): At the beginning of Mode 7, the third resonance begins. Then, the auxiliary switch S_3 turns on under the ZCS condition. The energy stored in the resonant capacitor C_r is transferred to the resonant inductor through auxiliary switch S_3. The auxiliary capacitor voltage v_{Ca} and resonant inductor current i_{Lr} can be derived from the Laplace transform, following Equations (32), (33), (35), and (36). Then, the equivalent circuit is shown in Figure 10. Mode 7 ends when the auxiliary capacitor C_a voltage reaches 0 V, as in Equation (38). The current that flows through the main inductor L_m increases linearly, as in Equation (31) and the energy is stored in the resonant inductor L_r through the auxiliary switch S_3. The i_{Lr} and v_{ca} values were defined by Equations (34) and (37).

$$i_{Lm}(t) = \frac{V_{in}}{L_m}t + I_{Lm6} \tag{31}$$

$$-\frac{Z_a I_{Lr4}}{s} = \frac{i_{Lr}(s)}{sC_a} + sL_r i_{Lr}(s) \tag{32}$$

$$i_{Lr}(s) = \frac{-\frac{Z_a I_{Lr4}}{L_r} \cdot \sqrt{L_r C_a} \cdot \frac{1}{\sqrt{L_r C_a}}}{s^2 + \left(\frac{1}{\sqrt{L_r C_a}}\right)^2} \tag{33}$$

$$i_{Lr}(t) = -I_{Lr4} sin\omega_a t \tag{34}$$

$$-C_a Z_a I_{Lr4} = v_{Ca}(s) sC_a + \frac{v_{Ca}(s)}{sL_r} \tag{35}$$

$$v_{Ca}(s) = -\frac{s}{s^2 + \left(\frac{1}{\sqrt{L_r C_a}}\right)^2} Z_a I_{Lr4} \tag{36}$$

$$v_{Ca}(t) = -Z_a I_{Lr4} cos\omega_a t \tag{37}$$

$$v_{Cr}(t) = 0 \tag{38}$$

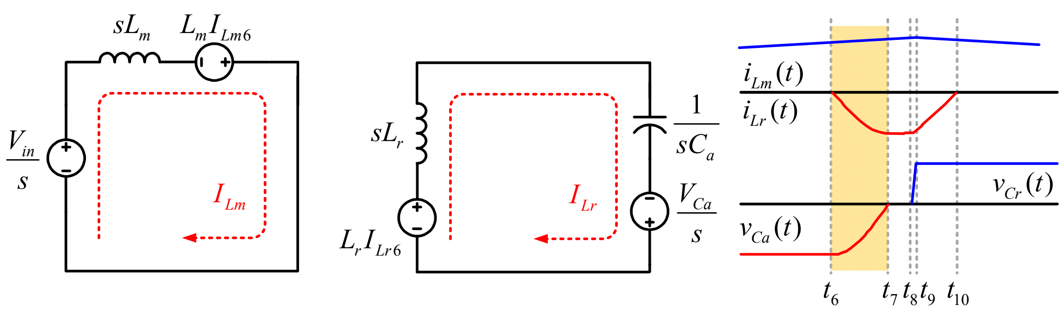

Figure 10. The equivalent circuit of Mode 7 and key waveform.

Mode 8 ($t_7 < t < t_8$): In Mode 8, the auxiliary capacitor voltage v_{Ca} becomes zero. Then, the main inductor current i_{Lm} increases linearly and the body diode of the auxiliary switch S_2 is turned on. The resonant inductor L_r current flows through the freewheeling path of the body diode—the main switch S_1. When the main switch S_1 is turned off, Mode 8 is complete. In this interval, the magnitude of the resonant inductor current i_{Lr} is equal to that of Mode 3. However, the current flow is reversed. The i_{Lm}, i_{Lr}, v_{Ca}, and v_{Cr} values are as follows in Equations (39) and (40):

$$i_{Lm}(t) = I_{Lm7} + \frac{V_{in}}{L}t,\ i_{Lr}(t_8) = i_{Lr7} \tag{39}$$

$$v_{Ca}(t) = 0,\ v_{Cr}(t) = 0 \tag{40}$$

The equivalent circuit of mode 8 and key waveform is shown Figure 11. The equivalent circuit is divided into main inductor current i_{Lm} and resonant inductor current i_{Lr}. The key waveform indicates i_{Lm}, i_{Lr}, v_{Ca}, and v_{Cr}.

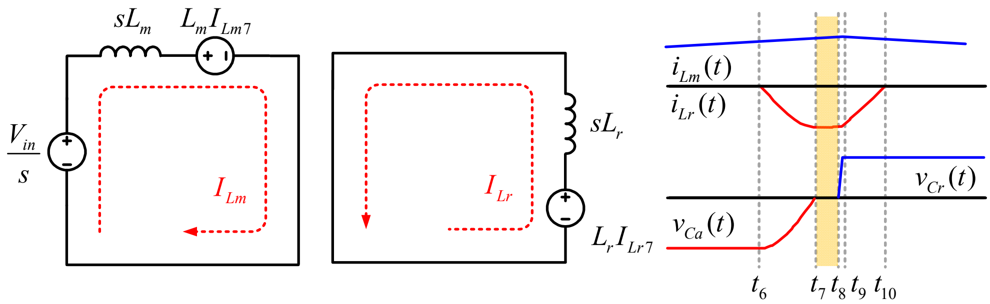

Figure 11. The equivalent circuit of Mode 8 and key waveform.

For Mode 9, the main and resonant current I_{Lm8} are defined by Equations (41) and (42).

$$i_{Lm}(t_8) = \frac{V_{in}}{L_m}t + I_{Lm7} = I_{Lm8} \tag{41}$$

$$i_{Lr}(t_8) = I_{Lr7} = I_{Lr8} \tag{42}$$

Mode 9 ($t_8 < t < t_9$): In this mode, the fourth resonance between the resonant inductor L_r and the resonant capacitor C_r begins. The current that flows in the resonance inductor L_r is reduced from the maximum point and the resonant capacitor C_r is charged by the total current of the main and resonant inductor. Then, the voltage of the resonant capacitor v_{Ca} is charged to the output voltage V_o, and Mode 9 ends. The resonant capacitor voltage v_{Ca} and resonant inductor current i_{Lr} can be derived from the Laplace transform, following Equations (44), (45), (47), and (48). The i_{Lm}, i_{Lr}, v_{Ca}, and v_{Cr} values are as follows in Equations (43), (46), (49), and (50):

$$i_{Lm}(t) = I_{Lm8} \tag{43}$$

$$-L_r(I_{Lr8}) = \frac{i_{Lr}(s)}{sC_r} + i_{Lr}(s)sL_r \tag{44}$$

$$i_{Lr}(s) = -\frac{s}{s^2 + \left(\frac{1}{\sqrt{L_r C_r}}\right)^2}(I_{L8}) \tag{45}$$

$$i_{Lr}(t) = I_{L8}cos\omega_r t \tag{46}$$

$$\frac{I_{L8}}{s} = \frac{v_{Cr}(s)}{sL_r} + v_{Cr}(s)sC_r \tag{47}$$

$$v_{Cr}(s) = \frac{\sqrt{\frac{L_r}{C_r}} \cdot \frac{1}{\sqrt{L_r C_r}}}{s^2 + \left(\frac{1}{\sqrt{L_r C_r}}\right)^2}(I_{L8}) \tag{48}$$

$$v_{Cr}(t) = Z_r I_{Lr8} sin\omega_r t \tag{49}$$

$$v_{Ca}(t) = 0 \tag{50}$$

The Mode 9 is divided into two equivalent circuits in Figure 12. Then, the equivalent circuit of resonance operation is shown. The key waveform of Mode 9 indicates i_{Lm}, i_{Lr}, v_{Ca}, and v_{Cr}. And the key waveform of Figure 12 shows the maximum of the main inductor current i_{Lm}.

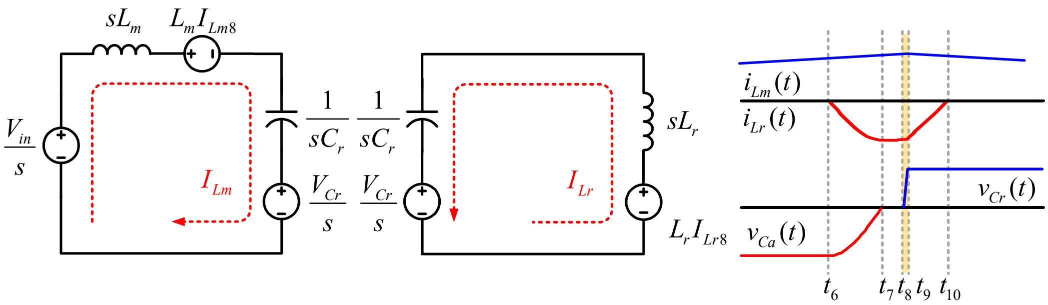

Figure 12. The equivalent circuit of Mode 9 and key waveform.

For Mode 10, the main inductor current I_{Lm9} is defined:

$$i_{Lm}(t_9) = I_{Lm8} = I_{Lm9} \tag{51}$$

Mode 10 ($t_9 < t < t_{10}$): The resonant inductor current i_{Lr} linearly decreases to zero. And if the resonant capacitor voltage v_{Ca} is charged with a larger output than output voltage V_o, then the output diode D_o is turned on. Mode 10 is completed, and the next switching cycle starts.

The Mode 10 is divided into two equivalent circuits in Figure 13. Then, the equivalent circuit of main inductor L_m is shown. Other equivalent circuit indicates resonant inductor L_r. The key waveform of Figure 13 shows the maximum of the main inductor current i_{Lm}. And resonant capacitors C_r are charged the output voltage.

$$i_{Lm}(t) = I_{Lm9} - \frac{V_o - V_{in}}{L}t \tag{52}$$

$$i_{Lr}(t) = I_{Lr9} - \frac{V_o}{L_r}t \tag{53}$$

$$v_{Cr}(t) = V_o,\ v_{Ca}(t) = 0 \tag{54}$$

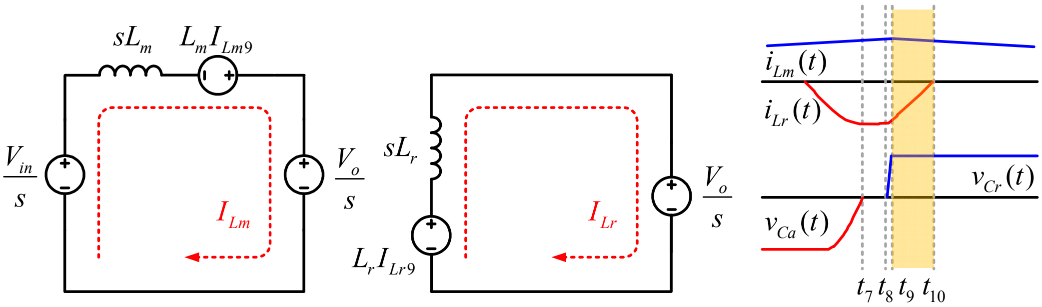

Figure 13. The equivalent circuit of Mode 10 and key waveform.

2.3. PWM Signal Analysis

PWM signals of the main and auxiliary switch are shown in Figure 14. The auxiliary switch S_2 is turned on before the main switch S_1 is turned on. Then turning on interval of the auxiliary switch S_2 can be divided into mode 2, mode 3 and mode 4. The main switch S_1 makes boost at turning on and turning off. The auxiliary switch S_3 operates to reduce conduction loss. And turning on interval of the auxiliary switch S_3 can be shown into mode 7.

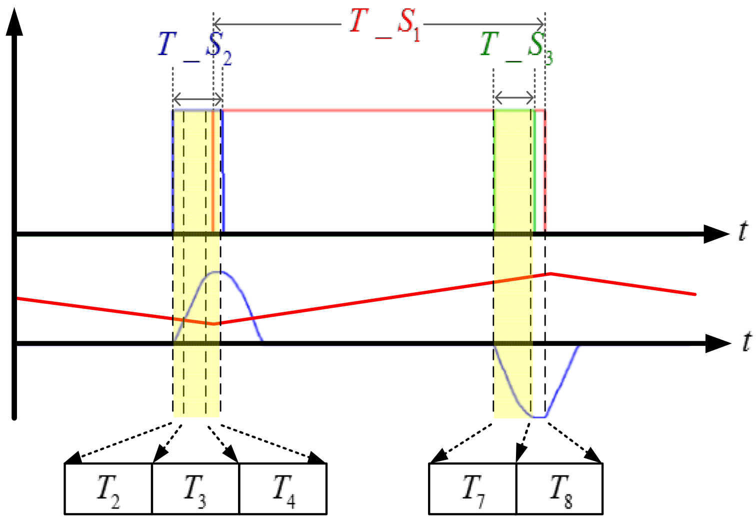

Figure 14. Pulse width modulation (PWM) signals of the main and auxiliary switch.

This design for a proposed resonant ZVT boost converter is composed of three switches, and the minimum turn-on and turn-off time should be satisfied in order to achieve ZVS and ZCS. The main switch controls the step-up ratio. Other auxiliary switches enable the main switch to operate with a soft switching. The resonances for the resonant inductor L_r and the resonant capacitor C_r are started by turning on the auxiliary switch S_2. When the charged energy completely discharges from the resonant capacitor, the main switch S_1 turns on in the ZVS condition. Before the main switch S_1 turns on, the auxiliary switch S_2 is turned on and turned off. To achieve the ZVS, a minimum time of auxiliary switch pulse width modulation (PWM) is required. The time is determined by Mode 2, Mode 3, and Mode 4. The T_2, T_3, and T_4 time must be satisfied according to the following equation:

$$T_2 = \frac{-I_{Lm.1}L_mL_r}{V_{in}L_r - V_o(L_m + L_r)} \tag{55}$$

$$T_3 = \frac{\sin^{-1}(\sin \omega_r t)}{2\pi F_r} \tag{56}$$

$$F_r = \frac{1}{2\pi\sqrt{L_rC_r}} \tag{57}$$

T_4 is determined by using a factor of k from the time delay of the switching elements.

$$T_4 = t \times k \tag{58}$$

$$t < \frac{L_m(I_{Lr3} - I_{Lm3})}{V_{in}} \tag{59}$$

The turning on and off times for the auxiliary switch S_2 can be satisfied, as shown in the following Equation (60):

$$T_{S2} > T_2 + T_3 + T_4 \tag{60}$$

Before the main switch is turned off, the auxiliary switch S_3 is turned on and off. After the energy for the resonant inductor L_r discharges and reaches zero, the auxiliary switch S_3 turns on. The auxiliary switch S_3 turns on in the ZCS condition. After the auxiliary capacitor C_a discharges, the auxiliary switch S_3 turns off in the ZVS condition. The turning on and off times for the auxiliary switch S_3 can be calculated by using the equations for Modes 7 and 8. T_7 requires a longer time than half the secondary resonant auxiliary frequency and T_8 requires a longer time than the off-delay time of the elements, which can be obtained from the manufacturer's data sheet. The shortest time for the auxiliary switch S_3 should be satisfied by using the following Equations (61)–(63).

$$T_7 = \frac{T_r}{2} = \pi\sqrt{L_r C_a} \tag{61}$$

$$T_8 > t_{d(off)} \tag{62}$$

$$T_{S3} > T_7 + T_8 \tag{63}$$

2.4. Resonant Device Design

Resonant capacitor C_r influences the ZVS operation of the main switch S_1. The ZVS switching process can be performed when the resonant capacitor C_r is sufficiently charged [16]. Thus, the design of resonant capacitors C_r is important. When the resonant capacitor C_r is charged and discharged in Mode 3 and Mode 9, the resonant time between the resonant inductor L_r and resonant capacitor C_r can be expressed as the following equation:

$$T_{mode3} = \frac{\pi}{2}\sqrt{L_r C_r} \tag{64}$$

In Mode 9, resonant capacitor C_r is charged to output voltage and can be expressed as the following equation:

$$T_{mode9} = C_r \frac{V_o}{2I_{in\_max}} \tag{65}$$

Assume that the maximum current of the resonant inductor is I_{in_max}, and the sum of the two inductor currents is the charging current of the resonant capacitor C_r. When Mode 9 is longer than Mode 3, the defective duty ratio is lower. Thus, the time is chosen as 0.1 T_s. The sum of Mode 3 and Mode 9 is selected as 1/10 of one cycle. The charging time of the resonant capacitor C_r must be longer for ZVS of the main switch. For this reason, the value of the resonant capacitor C_r should be chosen to be 15 times larger than that of the output switch capacitor. According to the output capacitance of main switch S_1, a suitable value of the resonant capacitor is 0.6 nF. The output capacitance of the main switch S_1 is given in the manufacturer's data sheet. As a result, resonant capacitor C_r used 10 nF to consider a margin of error.

$$\frac{\pi}{2}\sqrt{L_r C_r} + C_r \frac{V_o}{2I_{in\_max}} \leq 0.1 T_s \tag{66}$$

In addition, the resonant current between the resonant inductor L_r and resonant capacitor C_r charges the auxiliary capacitor C_a. The resonant time between the resonant inductor L_r and auxiliary capacitor C_a in Mode 5 and Mode 7 is set as one-fifth of the total turning on time. If the charging voltage of this resonant capacitor C_r is too large, it may be voltage stress. The auxiliary capacitance was calculated to be 39 nF. The auxiliary capacitor used 40 nF to consider a margin of error.

Resonance between resonant inductor L_r and capacitor C_r operates for soft switching of the main switch. Then, the main switch S_1 has satisfied the ZVT condition. Resonance design is very important to satisfy ZVS, ZCS, and ZVT [17]. But if the resonant inductor current i_{Lr} continues to increase linearly, the magnetic flux of the inductor is saturated [18]. Thus, the flux of the inductor must be prevented from reaching saturation, using the auxiliary capacitor C_a. The auxiliary capacitor C_a is charged from the negative current of the resonant inductor. In this case, energy relation can be defined by auxiliary capacitor C_a and resonant inductor L_r. Therefore, stored energy of the inductor is equal to or greater than the stored energy of the capacitor.

The resonant capacitor L_r must charge below the output voltage V_o. Obtained values in each mode can be expressed by the following Equations (67) and (68) [19–21]:

$$\frac{1}{2}L_r I_{Lr\_max}^2 \geq \frac{1}{2}C_a V_o^2 \tag{67}$$

$$C_a \leq \frac{L_r I_{Lr\_max}^2}{V_o^2} \tag{68}$$

3. Simulation Results

The computer was simulated to verify the operation of the new ZVT boost converter design. The design specifications of the elements used in the simulation are shown in Table 1. This paper tested the proposed converter by POWERSIM Inc. PSim9.2 software. The simulation time step has 1E-007 for detailed waveform analysis. The design specifications of the elements used in the simulation are shown in Table 1. The simulation was performed under a 30-kHz switching frequency and a 200–380 V voltage.

Table 1. Parameter of the proposed zero voltage transition (ZVT) converter.

Parameter	Symbol	Value	Parameter	Symbol	Value
Input Voltage	V_{in}	200 V	Main Inductor	L_m	1 mH
Output Voltage	V_o	380 V	Resonant Inductor	L_r	35 uH
Rated Power	P	4 kW	Resonant Capacitor	C_r	10 nF
Switching Frequency	f_s	30-kHz	Auxiliary Capacitor	C_a	40 nF

The waveform of each PWM signal is shown in Figure 15 and the resonant inductor current i_{Lr} flows according to each PWM signal.

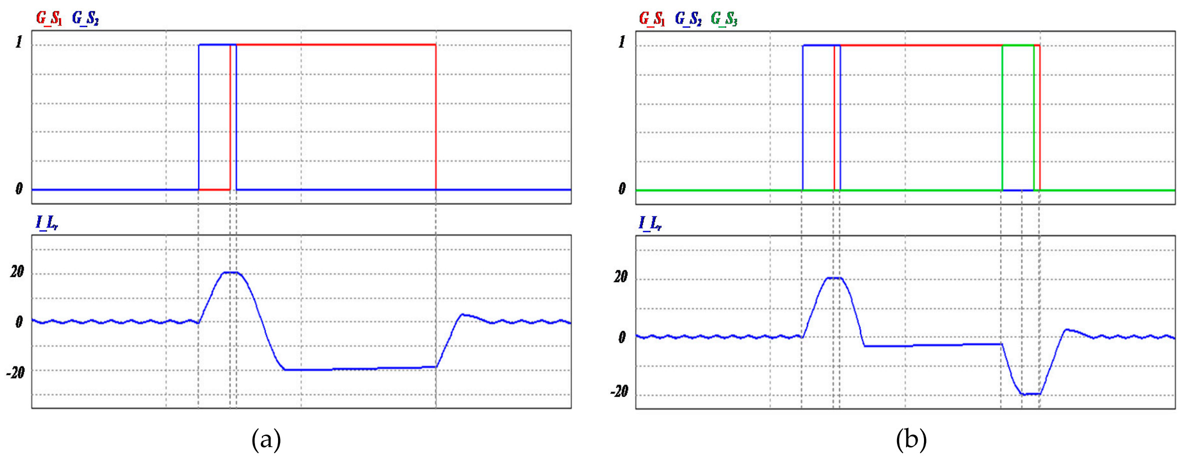

Figure 15. Waveforms of PWM signal and resonant inductor current. (**a**) Conventional converter and (**b**) proposed converter.

The current conduction period of the proposed converter is shorter than the conventional converter. The waveforms of the voltage and current of each switch are shown in Figure 16. The soft switching operations of each switch were successfully performed, as shown in Figure 16b. It also shows some voltage ringing, due to the resonance between the auxiliary switches S_2 and S_3. The switch used in the simulation is non-ideal, and the parasitic capacitances may cause a switch failure. Specifically, the output capacitance resonates with the resonance inductor and leads to ringing. These resonances may cause the current or voltage stress on the devices and finally increase the voltage rating of the devices.

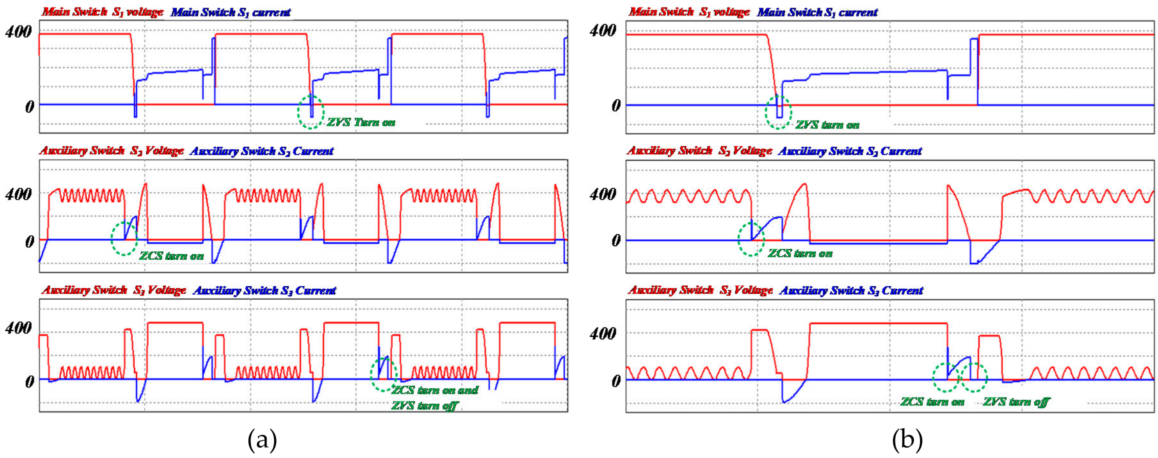

Figure 16. (**a**) Waveforms of voltage and current of each switch and (**b**) expansion waveforms.

Figure 17 shows the waveforms of the input and output of the voltage and current. The proposed ZVT boost converter can be applied to the photovoltaic system of DC distribution. Therefore, the output of the proposed converter can be directly connected to the DC voltage of the DC distribution building.

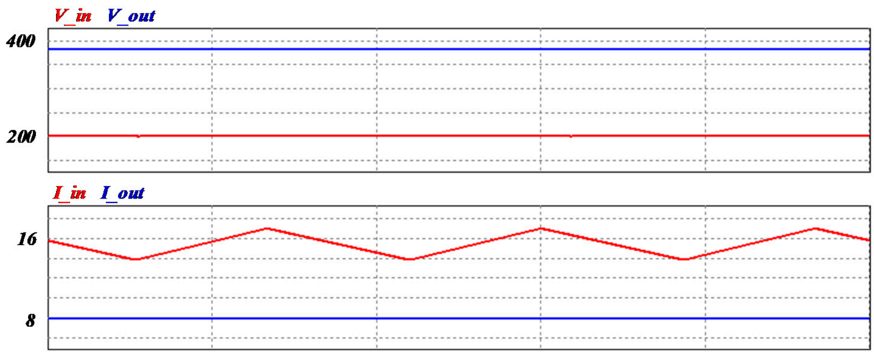

Figure 17. Waveforms of input/output voltage and current.

4. Experimental Results

In order to prove the theoretical analysis, experiments were conducted on the proposed ZVT boost converter in Figure 18. It consists of a boost converter, a controller, and a gate driver. The controller used in this experiment was the DSP TMS320F28335 from TI.

The experiment was conducted with the 4 kW, 30 kHz converter, which steps up the voltage from 200 V to 380 V.

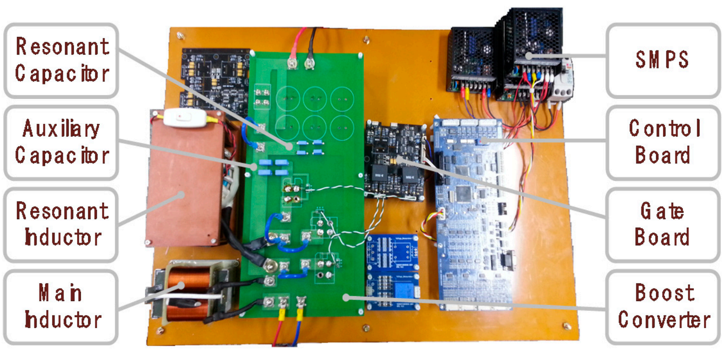

Figure 18. Experimental setup.

To compare the conventional and the proposed converter, current waveforms of the main inductor and the resonant inductor are shown in Figure 19. When the main switch S_1 is turned on, the current through the main inductor L_m increases linearly. When the main switch S_1 is turned off, the energy that was stored in the main inductor L_m is released through the output diode D_o and is transferred to the load. The same kinds of waveforms are shown in Figure 2. Conduction periods of the conventional converter were observed to be larger than those for the proposed converter.

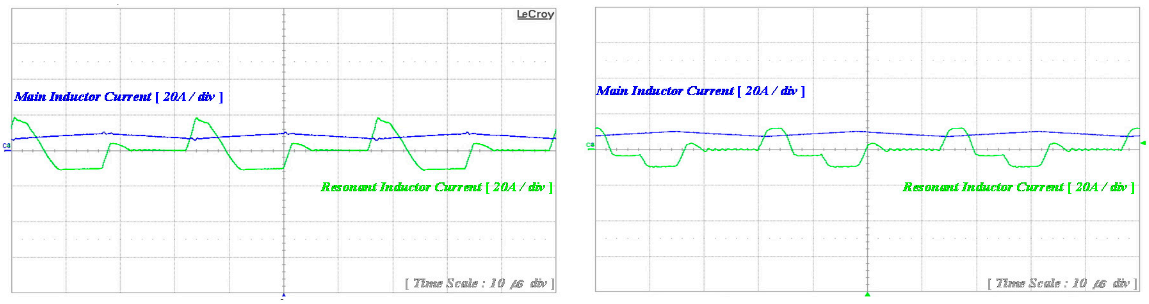

(a) (b)

Figure 19. Waveforms of main and resonant inductor current. (**a**) Conventional converter and (**b**) proposed converter.

The waveforms for the voltage and current across the main switch S_1 are shown in Figure 20. Before the main switch S_1 is turned on, the body diode of the main switch has a freewheeling period. Then, the main switch is turned on under ZVS in the ZVT condition. The waveforms for the voltage and current across the main switch S_1 are shown in Figure 20. Figure 20b is a close up of the soft switching in voltage and current of the main switch S_1.

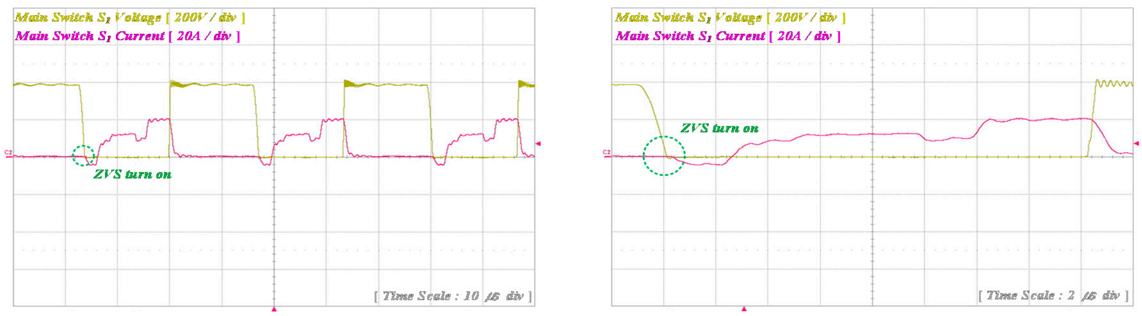

(a) (b)

Figure 20. (**a**) Waveforms of main switch S_1 voltage and current and (**b**) expansion waveforms of S_1.

The waveforms for the voltage and the current across the auxiliary switch S_2 are shown in Figure 21. The auxiliary switch S_2 is turned on under the ZCS condition because of the resonant inductor. Thus, the current of the auxiliary switch S_2 increases linearly from zero. The voltage of the auxiliary switch S_2 is equal to zero and the auxiliary capacitor Ca does not affect the auxiliary switch S_2. Thus, the waveforms of the auxiliary switch S_2 are shown by a negative resonant inductor auxiliary capacitor and a resonant operation. Figure 21b shows an extension of the soft switching of the auxiliary switch S_2.

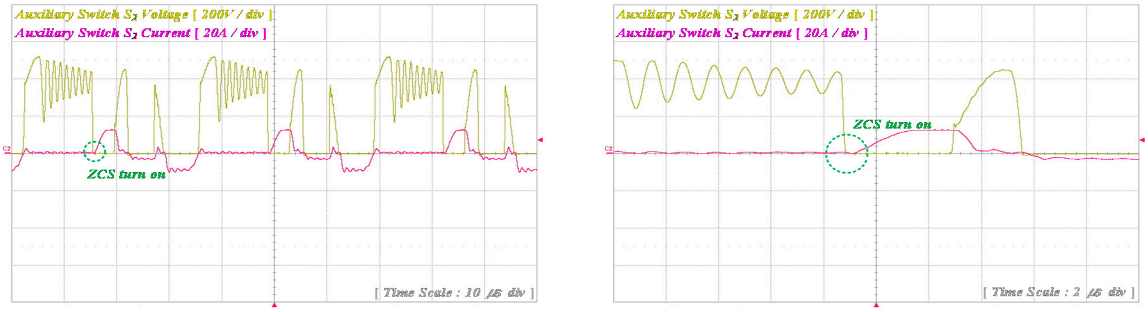

(a) (b)

Figure 21. (**a**) Waveforms of auxiliary switch S_2 voltage and current and (**b**) expansion waveforms of S_2.

Figure 22 shows the waveforms for the voltage and current across the auxiliary switch S_3. The body diode of the main switch is turned on under a zero-voltage switching condition. Afterwards, the auxiliary switch S_3 is turned on under the ZCS condition because of the resonant inductor L_r and auxiliary capacitor C_a. Then, voltage of the auxiliary switch S_3 remains at zero. Figure 22b shows the extension of soft-switching for the auxiliary switch S_3. Voltage ringing occurs due to the resonance between the auxiliary switches S_2 and S_3. The switch used in the simulation is non-ideal, and the parasitic capacitances may cause a switch failure. Specifically, the output capacitance resonates with the resonance inductor and leads to ringing.

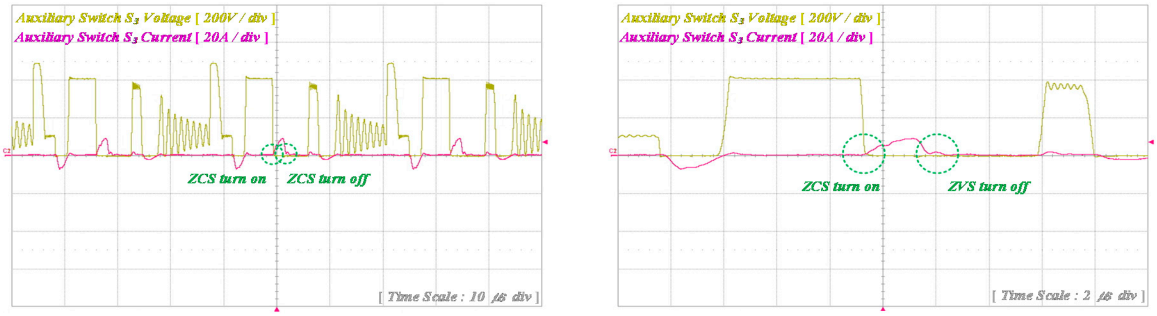

(a) (b)

Figure 22. (**a**) Waveforms of auxiliary switch S_3 voltage and current and (**b**) expansion waveforms of S_3.

The input/output voltage and current waveforms are shown in Figure 23. A voltage step-up occurs from an input voltage of 200 V to an output voltage of 380 V, indicating good control of the output voltage.

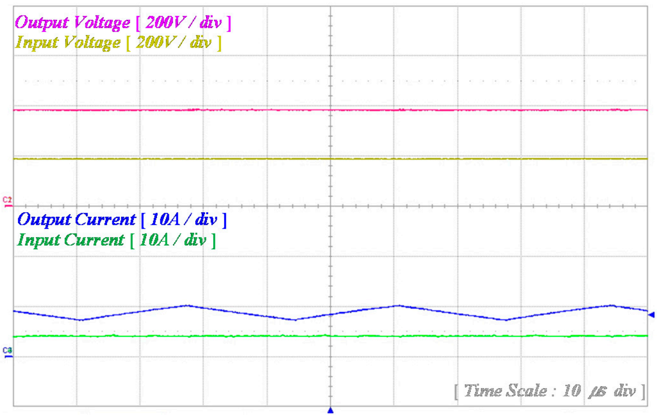

Figure 23. Waveforms of input/output voltage and current.

The efficiency comparison of the conventional (C) and proposed (P) converter is shown in Table 2. A power analyzer (model WT-3000) was used to confirm the efficiency of the proposed converter. The output power 380 V and the input power 200 V were fixed while measuring variable loads, based on a rated capacity of 4 kW. According to the efficiency measurements, a measured full-load efficiency of over 90% was confirmed, and a maximum efficiency of 96.5% was measured at 95% load.

Table 2. Efficiency comparison of conventional and proposed converter.

Load [%]		V_{in} [V]	I_{in} [A]	V_o [V]	I_o [A]	W_{in} [W]	W_o [W]	Efficiency [%]
28%	C	196.4	6.03	387.5	2.7	1184.29	1046.25	88.34
	P	201.4	5.4	387.5	2.53	1087.56	980.38	90.14
55%	C	200.8	11.27	384.9	5.3	2263.02	2039.97	90.14
	P	196.5	11.27	386.2	5.3	22.14.56	2046.86	92.43
76%	C	198.7	15.57	386.6	7.32	3093.76	2829.91	91.47
	P	181.7	16.57	386.4	7.32	3010.77	2828.45	93.94
95%	C	199.2	19.11	385.1	9.32	3806.71	3589.13	94.48
	P	189.9	19.86	384.4	9.45	3772.8	3642.03	96.53

5. Conclusions

In this paper, the resonant ZVT boost DC–DC converter, which uses the auxiliary resonant circuit, is proposed. All switches of the proposed converter were operated under ZVS and ZCS. Thus, the switching losses were reduced by using the resonant circuit. It is composed of two switches, the resonant inductor and two resonant capacitors. Furthermore, the proposed converter reduces the conduction loss of the resonant inductor, compared to the conventional converter. As a result, the proposed converter improves the whole system's efficiency better than the conventional converter at the same frequency. To verify, the experiment was successful. The measured efficiency of the proposed converter is 96.5%, which is a highly improved result, compared to the conventional resonant converter at 94.2%. In addition, based on mathematical modeling, the equivalent circuit of each operation mode was analyzed. Operation modes were divided, considering the current and voltage waveforms. The simulation was performed to verify the validation of the proposed converter. To conclude, the simulation and experimental results were the same.

Therefore, the proposed high-efficiency converter is suitable for applications such as photovoltaic converters of DC distribution and sensor systems.

Author Contributions: Conceptualization, H.J.L. and Y.-H.K.; Formal Analysis, H.J.L.; Supervision, Y.-H.K.

Funding: This research received no external funding.

Conflicts of Interest: The authors declare no conflict of interest.

Nomenclature

L_m	Main Inductor
L_r	Resonant Inductor
C_r	Resonant Capacitor
C_a	Auxiliary Capacitor
D_o	Output Diode
S_1	Main Switch
S_2	Auxiliary Switch 2
S_3	Auxiliary Switch 3
i_{Lm}	Main Inductor Current
i_{Lr}	Resonant Inductor Current
v_{Cr}	Resonant Capacitor Voltage
v_{Ca}	Auxiliary Capacitor Voltage
i_{Do}	Output Diode Current

References

1. Tsai, C.H.; Su, J.Y. A Soft-Switching SEPIC with Multi-Output Sources. *Electronics* **2017**, *6*, 35. [CrossRef]
2. Lin, B.-R. Investigation of a Resonant dc–dc Converter for Light Rail Transportation Applications. *Energies* **2018**, *11*, 1078. [CrossRef]
3. Lee, H.J.; Shin, S.C.; Hong, S.J.; Hyun, S.W.; Lee, J.H.; Won, C.Y. Performance Improvement of Isolated High Voltage Full Bridge Converter Using Voltage Doubler. *J. Electr. Eng. Technol.* **2014**, *9*, 2224–2236. [CrossRef]
4. Kim, Y.H.; Ji, Y.H.; Kim, J.G.; Jung, Y.C.; Won, C.Y. A New Control Strategy for Improving Weighted Efficiency in Photovoltaic AC Module-Type Interleaved Flyback Inverters. *IEEE Trans. Power Electron.* **2013**, *28*, 2688–2699. [CrossRef]
5. Kim, Y.H.; Jang, J.W.; Shin, S.C.; Won, C.Y. Weighted-Efficiency Enhancement Control for a Photovoltaic AC Module Interleaved Flyback Inverter Using a Synchronous Rectifier. *IEEE Trans. Power Electron.* **2014**, *29*, 6481–6493. [CrossRef]
6. Xue, J.; Lee, H. Enabling High-Frequency High-Efficiency Non-Isolated Boost Converters With Quasi-Square-Wave Zero-Voltage Switching and On-Chip Dynamic Dead-Time-Controlled Synchronous Gate Drive. *IEEE Trans. Power Electron.* **2015**, *30*, 6817–6828. [CrossRef]
7. Moshirvaziri, M.; Li, C.; Trescases, O. A quasi-resonant bi-directional tri-mode DC-DC converter with limited valley current. In Proceedings of the Twenty-Seventh Annual IEEE Applied Power Electronics Conference, Coronado, CA, USA, 5–9 February 2012; pp. 517–523. [CrossRef]
8. Liu, Y.C.; Chen, M.C.; Yang, C.Y.; Kim, K.A.; Chiu, H.J. High-Efficiency Isolated Photovoltaic Micro inverter UsingWide-Band Gap Switches for Standalone and Grid-Tied Applications. *Energies* **2018**, *11*, 569. [CrossRef]
9. Pilawa-Podgurski, R.C.N.; Sagneri, A.D.; Rivas, J.M.; Anderson, D.I.; Perreault, D.J. Very High Frequency Resonant Boost Converters. In Proceedings of the IEEE 38th Annual Power Electronics Specialists Conference, Orlando, FL, USA, 17–21 June 2007; pp. 2718–2724. [CrossRef]
10. Cheng, X.F.; Zhang, Y.; Yin, C. A ZVS Bidirectional Inverting Buck-Boost Converter Using Coupled Inductors. *Electronics* **2018**, *7*, 221. [CrossRef]
11. Urgun, S. Zero-voltage transition–zero-current transition pulse width modulation DC–DC buck converter with zero-voltage switching-zero-current switching auxiliary circuit. *IET Power Electron.* **2012**, *5*, 627–634. [CrossRef]
12. Mahesh, M.; Panda, A.K. High-power factor three-phase ac–dc soft-switched converter incorporating zero-voltage transition topology in modular systems for high-power industry applications. *IET Power Electron.* **2011**, *4*, 1032–1042. [CrossRef]
13. Phattanasak, M. A ZVT boost converter using an auxiliary resonant circuit. In Proceedings of the Power Electronics, Drives and Energy Systems, New Delhi, India, 12–15 December 2006; pp. 1–6. [CrossRef]
14. Khorasani, R.R.; Adib, E.; Farzanehfard, H. ZVT Resonant Core Reset Forward Converter with a Simple Auxiliary Circuit. *IEEE Trans. Ind. Electron.* **2018**, *65*, 242–250. [CrossRef]
15. Park, S.H.; Park, S.R.; Yu, J.S.; Jung, Y.C.; Won, C.Y. Analysis and design of a soft-switching boost converter with an HI-bridge auxiliary resonant circuit. *Trans. Power Electron.* **2010**, *25*, 2142–2149. [CrossRef]
16. Han, D.W.; Lee, H.J.; Shin, S.C.; Kim, J.G.; Jung, Y.C.; Won, C.Y. A new soft switching ZVT boost converter using auxiliary resonant circuit. In Proceedings of the IEEE Vehicle Power and Propulsion Conference, Seoul, Korea, 9–12 October 2012; pp. 1250–1255. [CrossRef]
17. Mercorelli, P.; Werner, N. An Adaptive Resonance Regulator Design for Motion Control of Intake Valves in Camless Engine Systems. *IEEE Trans. Ind. Electron.* **2017**, *64*, 3413–3422. [CrossRef]
18. Schimmack, M.; Costa, M.L.; Mercorelli, P. Comparing Two Voltage Observers in a Sensorsystem using Repetitive Control. *IFAC-PapersOnLine* **2016**, *49*, 7–11. [CrossRef]
19. Bodur, H.; Bakan, A.F. A new ZVT-PWM DC-DC converter. *IEEE Trans. Power Electron.* **2002**, *17*, 40–47. [CrossRef]
20. Aksoy, I.; Bodur, H.; Bakan, A.F. A new ZVT-ZCT-PWM DC-DC converter. *IEEE Trans. Power Electron.* **2010**, *25*, 676–684. [CrossRef]
21. Lee, D.Y.; Lee, M.K.; Hyun, D.S.; Choy, I. New Zero-Current-Transition PWM DC/DC Converters without Current Stress. *IEEE Trans. Power Electron.* **2002**, *18*, 95–104. [CrossRef]